Properties of Defect Modes of One-dimensional Quaternary Defective Photonic Crystal Nanostructure

Sofyan A. Taya *‡, Malek G. Daher *

*Physics Department, Islamic University of Gaza, P.O. Box 108, Gaza, Palestine

(staya@iugaza.edu.ps, malekjbreel20132017@gmail.com)

‡Corresponding Author; First Author, Postal address, Tel: +90 312 123 4567,

Fax: +90 312 123 4567, **staya@iugaza.edu.ps**

Received: 28.05.2022 Accepted:28.06.2022

Abstract- A defective quaternary photonic crystal having the $(ABCD)^N/F/(ABCD)^{N+1}$, where A, B, C and D are the photonic crystal layers, F is the defect layer and N is the number of periods, is investigated. We focus on the properties of the defect mode such as resonant wavelength, full width at half maximum, quality factor and maximum transmittance. These properties are examined with the variation of many parameters such as the incidence angle, the defect layer position and thickness and the number of periods. An angle of incidence of 85° and a number of periods of 9 can be considered as optimum since they correspond to the highest quality factor and the lowest full width at half maximum which enable the proposed photonic crystal to be efficiently used as an optical sensor and a filter.

Keywords: Quaternary photonic crystal, transfer matrix method, detect layer, transmission spectrum, defect mode

1. Introduction

Over the last two decades, many researchers have been studying photonic crystals, which are artificial dielectric or metallic structures whose refractive index changes periodically in space [1-6]. There are three types of photonic crystals, namely one-, two-, and three-dimensional periodic structures. Due to its simple design and theoretical modeling, one-dimensional photonic crystals have played a significant role among these groups. One-dimensional photonic crystals, which have been widely used in optics, have shown their promise in a variety of applications, including omnidirectional mirrors [7,8], low-threshold lasers [9], optical switching [10], modulators [11], tunable filters [12,13], etc. Photonic bandgaps [14] and defect modes [15] are considered the most important characteristics of photonic crystals. Due to the interference of waves encountering Bragg scattering due to perfect periodic lattices, some frequencies cannot travel through photonic crystals, the bandgap is then created. The manufactured photonic crystals are not completely defect-free, as they include some defect layers resulting in observing modes in the bandgap. Defect modes caused by defect layers in photonic crystals have many potential applications [16,17]. Therefore, it is very interesting to study the properties of defect modes in different types of photonic crystals [18-20]. These properties include resonant wavelength at which the defect mode occurs, full width at half maximum of the defect mode, quality factor and maximum transmittance. To the best of our knowledge, many research groups have examined both the bandgap and defect mode of binary and ternary photonic crystals with defect layers. Very few papers have discussed quaternary photonic crystals. Hollow-core Bragg fiber with quaternary photonic crystal cladding was proposed and fabricated [21]. The new cladding offers more design options. The transmission measurements revealed that it mainly uses higher-order photonic bandgaps to guide light [21]. The properties of the reflection phase in one-dimensional quaternary photonic crystals consisting of metamaterials and natural materials were investigated [22]. Two omnidirectional bandgaps were obtained in the proposed structure. It was observed that the value of the reflection phase difference between TE and TM waves can be controlled by

changing the incident angle and frequency [22]. The propagation of electromagnetic waves through a quaternary photonic crystal was analyzed [23]. The authors found that the transmission spectra increase with the continuous increase of the refractive index. The analysis was performed for TE waves [23]. Interface modes in a heterostructure composed of a quaternary photonic crystal were investigated [24]

Several papers have investigated defect modes in structures consisting of binary and ternary photonic crystals. Quaternary crystals are still relatively simple to fabricate while providing more interesting behavior compared to binary and ternary structures. The novelty of the current work is investigating the defect mode properties of a quaternary photonic crystal since to the best of our knowledge, no one has considered the defect modes of quaternary photonic crystals.

In this work, a defective quaternary photonic crystal is studied. Defect mode properties such as wavelength position, full width at half maximum, quality factor and maximum transmittance of the defect mode are investigated. The main goal of the current work is to study the tuning of the transmission spectrum of a defective quaternary photonic crystal. The importance of the present work is that the proposed photonic crystal can be as a tunable filter. Another significant application of the proposed structure is in the field of optical sensing. The proposed photonic crystal can be used in biosensing, chemical sensing and refractometric sensing.

2. Design and Theoretical Simulation

A one-dimensional quaternary defective photonic crystal is proposed. The photonic crystal has the structure $(ABCD)^N/F/(ABCD)^{N+1}$, where N is the number of periods. Layers A, B, C and D have thickness d_1, d_2, d_3, and d_4 and indices of refraction n_1, n_2, n_3 and n_4. F is the defect layer with a thickness d_f and an index n_f. The defect layer lies between N and N+1 periods. Fig. 1 shows a schematic diagram of the proposed quaternary defective photonic crystal. Here, we have used the well-known transfer matrix method to study the transmission spectra.

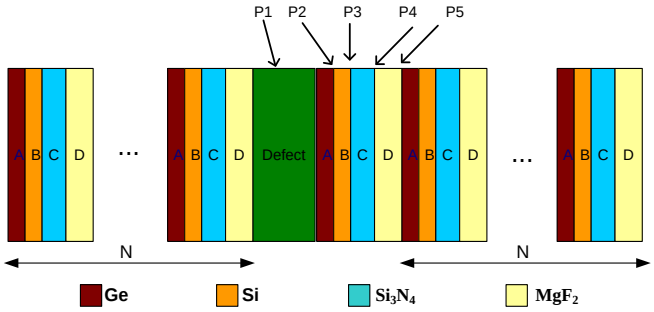

Fig. 1. Schematic diagram of a one-dimensional quaternary photonic crystal having a defect layer.

The transfer matrix method is appropriate and accurate for finite-size photonic bandgap structures with a defect layer. The characteristic transfer matrix for one layer is defined as [15]

$$G_j = \begin{bmatrix} cos(S_j) & -\frac{i\ sin(S_j)}{Y_j} \\ -i\ Y_j sin(S_j) & cos(S_j) \end{bmatrix} \quad (1)$$

S_j is the phase variation of the light wave propagating through the j[th] layer, where [14]

$$S_j = \frac{2\pi}{\lambda} n_j d_j \cos\theta_j \quad (2)$$

where n_j and d_j are the refractive index and thickness of the layer. θ_j is the angle of incidence of the layer which is given in terms of the initial incidence angle θ_0 as [15]

$$cos\,\theta_j = \sqrt{1 - \left(\frac{n_0\ sin(\theta_0)}{n_j}\right)^2} \quad (3)$$

$Y_j = n_j \cos(\theta_j)$ for transverse electric (TE) wave whereas $Y_j = \cos(\theta_j)/n_j$ for transverse magnetic (TM) wave and n_0 is the refractive index of the ambient medium. The transfer matrix G_0 of one period consisting of four layers *A*, *B*, *C* and *D* can be written as $G_0 = G_A\ G_B\ G_C\ G_D$. The full transfer matrix *G* of a defective quaternary photonic crystal can be expressed as [16]

$$G = (G_0)^N G_F (G_0)^N = \begin{bmatrix} G_{11} & G_{12} \\ G_{21} & G_{22} \end{bmatrix} \quad (4)$$

where G_F is the transfer matrix of the defect layer and G_{ij} are the elements of the total transfer matrix *G*. The transmission coefficient can be written as [15]

$$t = \frac{2Y_{in}}{(G_{11}+G_{12}\ Y_S)Y_{in}+(G_{21}+G_{22}\ Y_S)} \quad (5)$$

and the transmittance can have the form [15]

$$T = \frac{Y_S}{Y_{in}}|t|^2 \quad (6)$$

The reflection coefficient can be written as [16]

$$r = \frac{(G_{11}+G_{12}Y_S)Y_{in}-(G_{21}+G_{22}Y_S)}{(G_{11}+G_{12}Y_S)Y_{in}+(G_{21}+G_{22}Y_S)} \quad (7)$$

and the reflectance can have the form [14]

$$R = |r|^2 \quad (8)$$

For transverse electric (TE) waves, $Y_{in} = Y_s = \cos(\theta_0)$ since the quaternary photonic crystal is assumed to be surrounded by air. Based on the above equations, we can study the properties of defect modes of the defective quaternary photonic crystal.

3. Results and Discussion

The structure air/$(ABCD)^N$/F/$(ABCD)^{N+1}$/air is proposed as a one-dimensional quaternary defective photonic crystal. Layers A, B, C and D are taken as Ge ($n_1 = 4.23$), Si ($n_2 = 3.4$), Si_3N_4 ($n_3 = 2.0$) and MgF_2 ($n_4 = 1.37$), respectively. These layers have the thicknesses $d_1 = 41.43$ nm, $d_2 = 51.47$ nm, $d_3 = 87$ nm and $d_4 = 127.73$ nm, respectively. The thicknesses are determined according to the Bragg quarter-wave condition in which $d_i n_i = \lambda/4$. The defect layer refractive index is chosen as $n_f = 1.333$ and its thickness $d_f = 1D$, where $D = d_1 + d_2 + d_3 + d_4$. The defect layer (F) lies between N and N+1 periods where N = 5. Transverse electric (TE) waves are assumed in this paper.

The transmission spectrum is plotted in Fig. 2(a). The wavelength of the incident radiation is taken in the spectral range of 500 nm to 900 nm. In general, there are three windows of optical communications. The first optical window is centered at 850 nm and is used for multimode links. The second window is centered at 1310 nm and is used for single-mode links and wave division multiplexing. The third window (sometimes called C-band) is centered at 1550 nm and is used for single-mode links and dense wave division multiplexing. We have chosen the working spectral range of 500 – 800 nm because it is very common in such applications [15,16]. Normal incidence is first considered in which $\theta_0 = 0°$. A photonic bandgap of width 147.21 nm can be observed with left and right edges are at wavelengths of 628.23 nm and 775.44 nm, respectively. Fig. 2(b) shows an enlarged view of the defect mode which is found at a resonant wavelength of 658.17 nm. The full width at half maximum of the resonant peak is FWHM = 0.60 nm. The quality factor and maximum transmittance of the resonant peak are 1096.95 and 0.93, respectively.

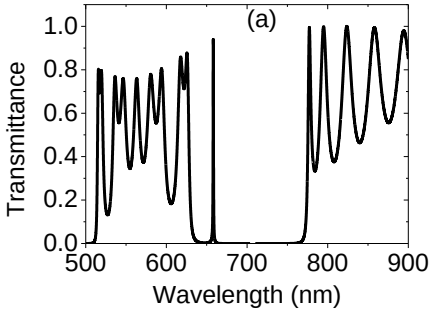

(a)

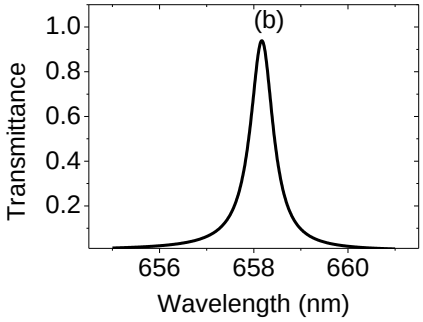

(b)

Fig. 2. (a) Transmission spectrum of a quaternary photonic crystal for TE wave. (b) An enlarged view of the defect mode ($\theta_0 = 0.0°$, $n_1 = 4.23$, $n_2 = 3.4$, $n_3 = 2.0$, $n_4 = 1.37$, $d_f = 1D$, N = 5 and the defect layer position is P1).

3.1 Effect of the Incident Angle

To examine the incident angle effect on the defect mode properties, the transmission spectra are investigated at different angles of incidence in Fig. 3. The defect mode shifts to a lower wavelength region as the incident angle increases. The Fig. shows a filter with different allowed wavelengths. The properties of these defect modes are presented in Table 1. The resonant wavelength, full width at half maximum, quality factor and maximum transmittance of the defect modes are all presented in Table 1 for different incident angles. The resonant wavelength variation as a function of the incident angle is shown in Fig. 4 (simulated data as red points). The relation between the resonant wavelength (RW) and the incident angle (θ_0) of the photonic crystal can be fitted by the following relation

$$RW(\theta_0) = 657.9 + 0.239\theta_0 - 0.0479\,{\theta_0}^2 + 3.465 \times 10^{-4}\,{\theta_0}^3 \quad (9)$$

which is plotted as a black curve in Fig. 4. The fitting equation (9) is helpful to find the resonant wavelength of the design at any incident angle located between $\theta_0 = 0°$ and $\theta_0 = 85°$. As shown in Fig. 4, the matching between the simulated data and the fitting curve is perfect. The incident angle has a significant influence on the defect mode width. The full width at half maximum has its highest value for normal incidence, as shown in Fig. 5. For angles greater than zero, the full width at half maximum starts declining which means a sharper defect mode. For applications such as optical sensing, a sharper defect mode is recommended. The relation between the full width at half maximum (FWHM) and the incident angle can be fitted by the following equation.

$$FWHM(\theta_0) = 0.6 + 19.5 \times 10^{-4}\,\theta_0 - 3.1 \times 10^{-4}\,{\theta_0}^2 + 8.17 \times 10^{-6}\,{\theta_0}^3 - 4.47 \times 10^{-8} \quad (10)$$

The fitting Eq. (10) can be used to predict the full width at half maximum of defect modes at any value of the incident angle in the range from $\theta_0 = 0.0°$ to $\theta_0 = 85°$. The fitting equation (Eq. 10) is plotted as a function of the incident angle (black curve) along with the simulated data (red points) in Fig. 5. The matching between the simulated data and the fitting relation is perfect.

The effect of the incident angle on the quality factor is shown in Fig. 6. The quality factor can be enhanced as the incident angle increases. For high incident angles such as $\theta_0 = 75°$ and $\theta_0 = 85°$, the quality factor shows a considerable growth to values of 1416.89 and 3636.4, respectively. In the applications of sensing, a high-quality factor is also needed so high incidence angles are desired. The relation between quality factor (QF) and the incident angle can be fitted by the following equation.

$$QF(\theta_0) = 1124.9 - 51.8\theta_0 + 4.4\,{\theta_0}^2 - 0.12{\theta_0}^3 + 7.66 \times 10^{-4}{\theta_0}^4 \quad (11)$$

The fitting equation of the quality factor as a function of the incident angle (black curve) along with the simulated data (red points) are shown in Fig. 6.

Fig. 7 shows a linear variation of the defect mode maximum transmittance with the incidence angle. Generally, a high transmittance close to unity is obtained for all incident angles. As the incident angle changes from $\theta_0 = 0.0°$ to $\theta_0 = 85°$, the maximum transmittance enhances from 0.93 to 1.00. The relation between the maximum transmittance (MT) and the incident angle can be fitted by the following linear equation.

$$MT(\theta_0) = 0.92854 + 8.39416 \times 10^{-4}\,\theta_0 \quad (12)$$

There is an acceptable matching between the simulated data (red points) and the fitted linear equation (black curve) as shown in Fig. 7. An angle of incidence of 85° nm can be considered as optimum since it has the highest quality factor, the lowest full width at half maxim and a maximum of transmittance of unity.

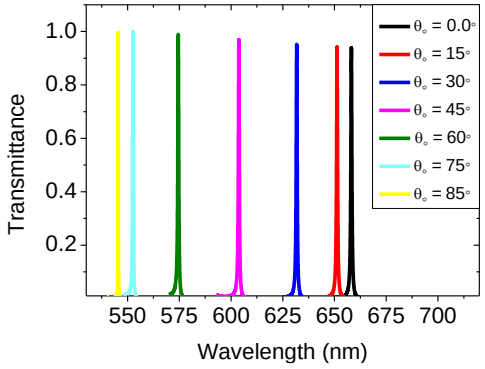

Fig. 3. Transmission spectra of a quaternary photonic crystal for different incident angles at $n_1 = 4.23$, $n_2 = 3.4$, $n_3 = 2.0$, $n_4 = 1.37$, $d_f = 1D$, N = 5 and the defect layer position is P1.

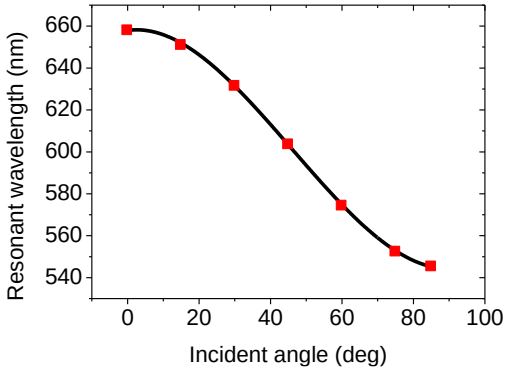

Fig. 4. Resonant wavelength of the defect mode as a function of the incident angle at $n_1 = 4.23$, $n_2 = 3.4$, $n_3 = 2.0$, $n_4 = 1.37$, $d_f = 1D$, N = 5 and the defect layer position is P1.

Table 1. Resonant wavelength, full width at half maximum, quality factor and maximum transmittance of the defect mode for different incident angles.

Incident angle (deg)	Resonant wavelength (nm)	FWHM (nm)	Quality factor	Maximum transmittance
0.0	658.17	0.60	1096.95	0.93
15	651.24	0.58	1122.82	0.94
30	631.73	0.55	1148.6	0.95
45	603.77	0.53	1139.18	0.97
60	574.5	0.52	1104.80	0.98
75	552.59	0.39	1416.89	0.99
85	545.46	0.15	3636.4	1.0

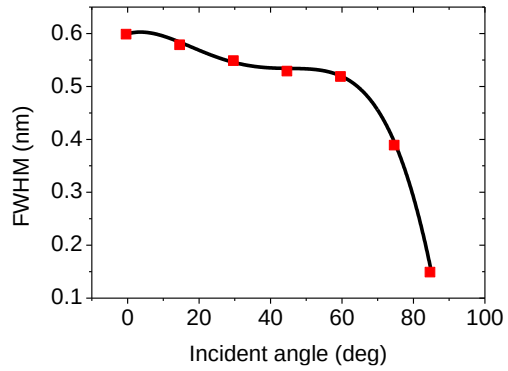

Fig. 5. Full width at half maximum versus the incident angle at $n_1 = 4.23$, $n_2 = 3.4$, $n_3 = 2.0$, $n_4 = 1.37$, $d_f = 1D$, N = 5 and the defect layer position is P1.

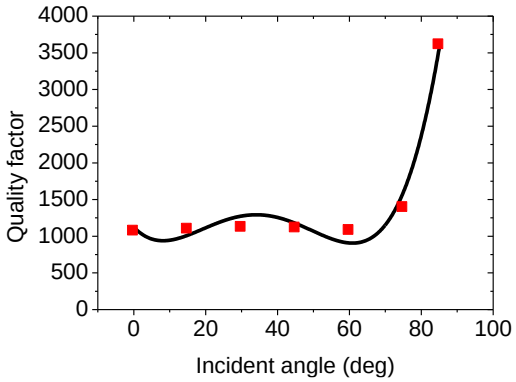

Fig. 6. Quality factor versus the incident angle at n_1 = 4.23, n_2 = 3.4, n_3 = 2.0, n_4 = 1.37, d_f = 1D, N = 5 and the defect layer position is P1.

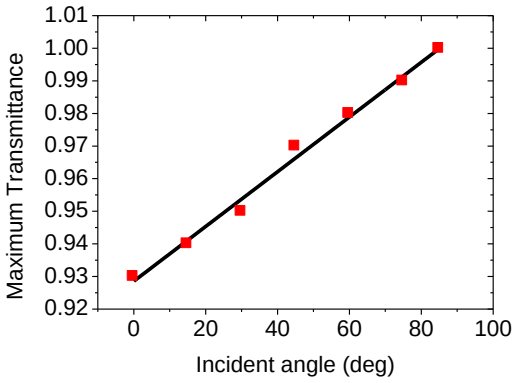

Fig. 7. Maximum transmittance versus the incident angle at n_1 = 4.23, n_2 = 3.4, n_3 = 2.0, n_4 = 1.37, d_f = 1D, N = 5 and the defect layer position is P1.

3.2 Effect of the Defect Layer Position

In this subsection, the influence of the defect layer position (P1, P2, P3, P4 or P5) on the defect mode properties is investigated. Positions P1, P2, P3, P4 and P5 mean that the photonic crystal has the structures $(ABCD)^N/F/(ABCD)^{N+1}$, $(ABCD)^N/AFBCD/(ABCD)^N$, $(ABCD)^N/ABFCD/(ABCD)^N$, $(ABCD)^N/ABCFD/(ABCD)^N$, $(ABCD)^{N+1}/F/(ABCD)^N$, respectively. The transmission spectra are investigated at different defect layer positions as shown in Fig. 8. The properties of the defect mode are presented in Table 2 for different positions of the defect layer. The variation of resonant wavelength as a function of the defect layer position is shown in Fig. 9. Position P2 shows the highest resonant wavelength whereas position P4 shows the lowest one. The full width at half maximum variation with different positions of the defect layer is shown in Fig. 10. Position P3 has the sharpest defect mode of width 0.38 nm. The variations of the quality factor and maximum transmittance with the positions of the defect layer are illustrated in Fig. 11 and Fig. 12, respectively. The position P3 seems optimum for optical sensing applications since it has the sharpest full width at half maximum (0.38 nm), high-quality factor (1746.5) and high transmittance (0.98).

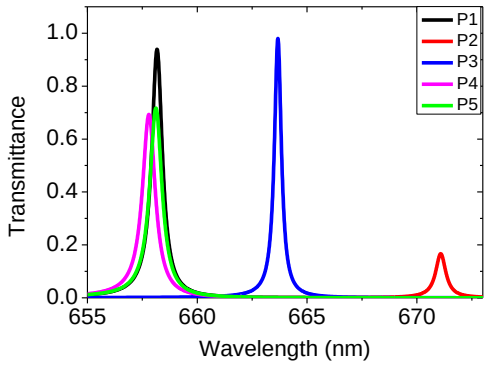

Fig. 8. Transmission spectra of a quaternary photonic crystal for different positions of the defect layer at n_1 = 4.2 n_2 = 3.4, n_3 = 2.0, n_4 = 1.37, θ_0 = 0.0°, d_f = 1D and N = 5.

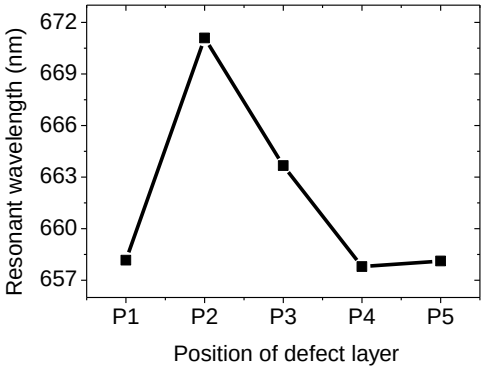

Fig. 9. Resonant wavelength of the defect mode as a function of the defect layer position at n_1 = 4.23, n_2 = 3.4, n_3 = 2.0, n_4 = 1.37, θ_0 = 0.0°, d_f = 1D and N = 5.

Table 2. Resonant wavelength, full width at half maximum, quality factor and maximum transmittance of the defect mode for different defect layer positions.

Defect layer position	Resonant wavelength (nm)	FWHM (nm)	Quality factor	Maximum transmittance
P1	658.17	0.60	1096.95	0.93
P2	671.09	0.55	1220.16	0.17
P3	663.67	0.38	1746.5	0.98
P4	657.8	0.70	939.71	0.69
P5	658.12	0.69	953.79	0.71

3.3 Effect of the Defect Layer Thickness

This subsection is devoted to investigating the effect of variation of defect layer thickness on the properties of the defect mode. Fig. 13 shows the transmission spectra of the quaternary PC at different defect layer thicknesses.

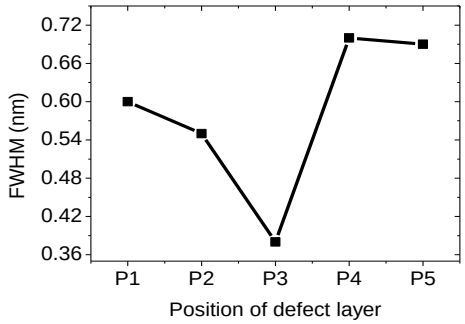

Fig. 10. Full width at half maximum versus the defect layer position at n_1 = 4.23, n_2 = 3.4, n_3 = 2.0, n_4 = 1.37, θ_0 = 0.0°, d_f = 1D and N = 5.

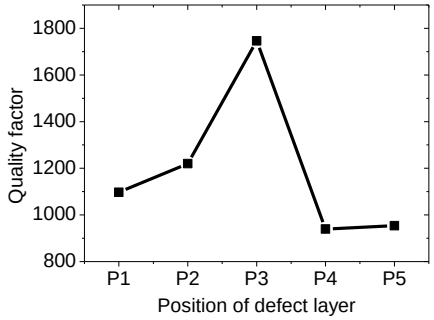

Fig. 11. Quality factor versus the defect layer position at n_1 = 4.23, n_2 = 3.4, n_3 = 2.0, n_4 = 1.37, θ_0 = 0.0°, d_f = 1D and N = 5.

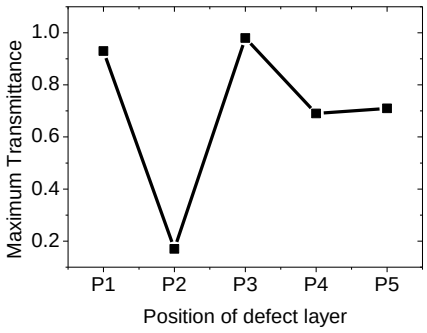

Fig. 12. Maximum transmittance versus the defect layer position at n_1 = 4.23, n_2 = 3.4, n_3 = 2.0, n_4 = 1.37, θ_0 = 0.0°, d_f = 1D and N = 5.

The defect layer thickness was varied from 307.63 nm to 520 nm and all the properties of the defect mode are determined. The defect mode shifts to a higher wavelength region as the defect layer thickness increases. The defect mode properties are presented in Table 3. The resonant wavelength as a function of the defect layer thickness is shown in Fig. 14 (red points). The relation between the resonant wavelength and the defect layer thickness (d_f) can be fitted by the following linear equation.

$$RW(d_f) = 511.87 + 47.583 \times 10^{-2}\, d_f \quad (13)$$

Fig. 14 shows a good matching between the simulated data (red points) and the fitted linear equation (black curve).

The standing wave formula, which is given by $\zeta = L\,\lambda = n_{eff}\,K$, can be used to explain the resonant peak dependency on the defect layer thickness, where ζ is the optical path, L is an integer, n_{eff} is the photonic crystal effective refractive index and K is the geometric path [25]. As the defect layer thickness increases, the geometric path increases and the resonant condition of the standing wave also increases. Hence, a redshift takes place to keep the optical path unchanged.

The variation of full width at half maximum shows that there is an optimum defect layer thickness of 400 nm at which the full width at half maximum is minimum (Fig. 15). The relation between the full width at half maximum and the defect layer thickness can be fitted by the following equation.

$$FWHM(d_f) = 55.91 - 0.532 d_f + 1.93 \times 10^{-3}\, {d_f}^2 - 3.146 \times 10^{-6}\, {d_f}^3 + 1.956 \times 10^{-9}\, {d_f}^4 \quad (14)$$

The fitting equation can predict the full width at half maximum at any defect layer thickness in the considered range. Fig. 15 shows both simulated data (red points) and fitted relation (black curve).

The quality factor increases as the defect layer thickness increases until it reaches its maximum value of 2810 at a thickness of 400 nm as shown in Fig. 16. For defect layer thickness greater than 400 nm, the quality factor starts to drop. The relation between the quality factor and the defect layer thickness can be fitted by the following equation.

$$QF(d_f) = 139179 - 1617.7\, d_f + 6.77\, {d_f}^2 - 12 \times 10^{-3}\, {d_f}^3 + 7.725 \times 10^{-6}\, {d_f}^4 \quad (15)$$

which is plotted as a black curve in Fig. 16.

The maximum transmittance as a function of the defect layer thickness is shown in Fig. 17. It exhibits a minimum value at a thickness of about 400 nm. For thicknesses greater and less than 400 nm, it increases. It exhibits its maximum value of 0.96 at a defect layer thickness of 500 nm. The relation between the maximum transmittance and the defect layer thickness can be fitted by the following equation.

$$MT(d_f) = 1.11 - 2.7 \times 10^{-4}\, d_f - 2.36 \times 10^{-6}\, {d_f}^2 + 4.5 \times 10^{-9}\, {d_f}^3 \quad (16)$$

Fig. 17 shows the fitted equation (black curve) and the simulated data (red points).

A defect layer thickness of 400 nm can be considered as optimum since it has the highest quality factor and the lowest full width at half maxim, especially for optical sensor applications.

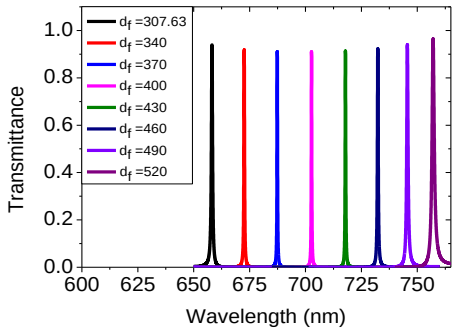

Fig. 13. Transmission spectra of a quaternary photonic crystal for different defect layer thicknesses at $n_1 = 4.23$, $n_2 = 3.4$, $n_3 = 2.0$, $n_4 = 1.37$, $\theta_0 = 0.0°$, N = 5 and the defect layer position is P1.

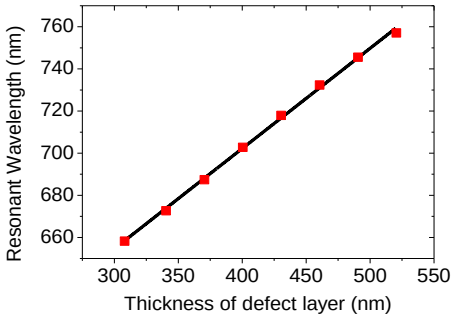

Fig. 14. Resonant wavelength of the defect mode as a function of the defect layer thickness at $n_1 = 4.23$, $n_2 = 3.4$, $n_3 = 2.0$, $n_4 = 1.37$, $\theta_0 = 0.0°$, N = 5 and the defect layer position is P1.

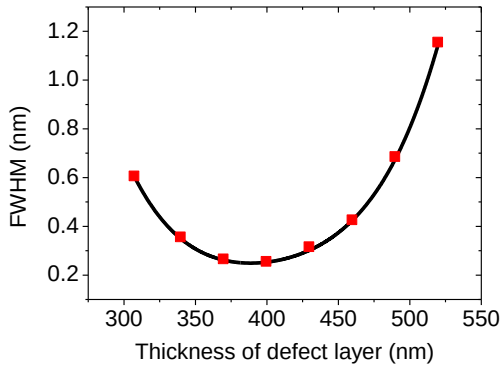

Fig. 15. Full width at half maximum versus the defect layer thickness at $n_1 = 4.23$, $n_2 = 3.4$, $n_3 = 2.0$, $n_4 = 1.37$, $\theta_0 = 0.0°$, N = 5 and the defect layer position is P1.

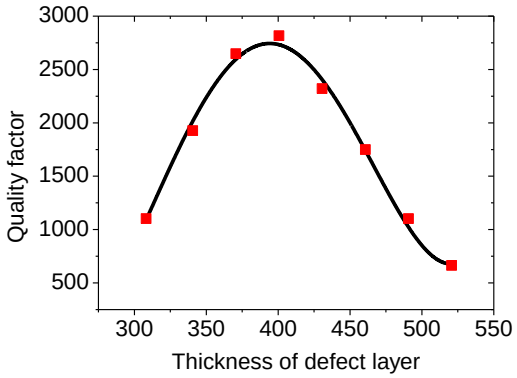

Fig. 16. Quality factor versus the defect layer thickness at $n_1 = 4.23$, $n_2 = 3.4$, $n_3 = 2.0$, $n_4 = 1.37$, $\theta_0 = 0.0°$, N = 5 and the defect layer position is P1.

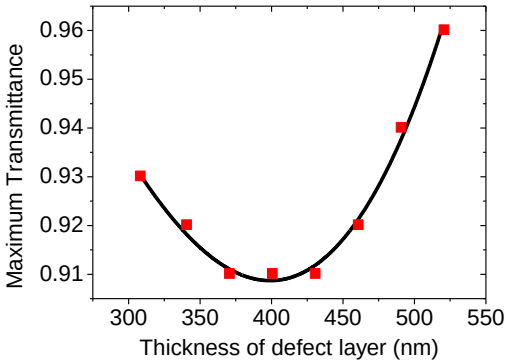

Fig. 17. Maximum transmittance versus the defect layer thickness at $n_1 = 4.23$, $n_2 = 3.4$, $n_3 = 2.0$, $n_4 = 1.37$, $\theta_0 = 0.0°$, N = 5 and the defect layer position is P1.

Table 3. Resonant wavelength, full width at half maximum, quality factor and maximum transmittance of the defect mode for different defect layer thicknesses.

Defect layer thickness (nm)	Resonant wavelength (nm)	FWHM (nm)	Quality factor	Maximum transmittance
307.63 (1D)	658.17	0.60	1096.95	0.93
340	672.59	0.35	1921.68	0.92
370	687.37	0.26	2643.73	0.91
400	702.69	0.25	2810.76	0.91
430	717.86	0.31	2315.67	0.91
460	732.32	0.42	1743.61	0.92
490	745.55	0.68	1096.39	0.94
520	757.05	1.15	658.30	0.96

3.4 Effect of the Number of Periods

In this subsection, the effect of the number of periods on the defect mode properties is investigated. The transmission spectra are investigated at different numbers of periods as shown in Fig. 18. The number of periods is varied between N = 3 and N = 9. The properties of the defect mode are presented in Table 4 for different numbers of periods. The defect mode position shows a barely detectable shift to a higher wavelength region as the number of periods changes from N = 3 to N = 9 as shown in Fig. 19. The resonant wavelength variation as a function of the number of periods (N) can be fitted by the following equation.

$$RW(N) = 642.81 + 8.5\,N - 1.77\,N^2 + 0.16N^3 - 5.68 \times 10^{-3}N^4 \quad (17)$$

The fitting equation is plotted in Fig. 19 as a black curve while the simulated data are shown as red points. Good matching can be seen between them.

The full width at half maximum exhibits a continuous decrease as the number of periods increases (Fig. 20). A full width at half maximum of 3.8 nm is obtained at N = 3 whereas a full width at half maximum of 0.02 nm is attained at N = 9. A very sharp peak is observed at N = 9 that is recommended for the optical sensing field. The relation between the full width at half maximum and the number of periods can be fitted by the following equation.

$$FWHM(N) = 30.7 - 17.05\,N + 3.6\,N^2 - 0.34\,N^3 + 12 \times 10^{-3}\,N^4 \quad (18)$$

Fig. 20 shows a well matching between the simulated data (red points) and the fitted relation (black curve). Fig. 21 shows the continuous increase of the quality factor with the increase of the number of periods. It starts at a value of 172.74 at N = 3 and rapidly increases to a value of 32925.5. The relation between the quality factor and the number of periods can be fitted by the following equation.

$$QF(N) = -12976 + 8224.5\,N - 1371\,N^2 - 15.3\,N^3 + 14.354\,N^4 \quad (19)$$

The fitting relation is also shown in Fig. 21. The maximum transmittance doesn't show a significant dependence on the number of layers (Fig. 22). It is constant until the number of periods reaches 7, then it exhibits a little decline and reaches 0.90 at N = 9. The relation between maximum transmittance and the number of periods can be fitted by the following equation.

$$MT(N) = 0.91 + 0.018N - 0.007N^2 + 12.63 \times 10^{-4}\,N^3 - 7.6 \times 10^{-5}\,N^4 \quad (20)$$

The black curve of Fig. 22 shows the fitting equation. A number of layers of 9 can be considered as optimum since it corresponds to the highest quality factor and the lowest full width at half maximum.

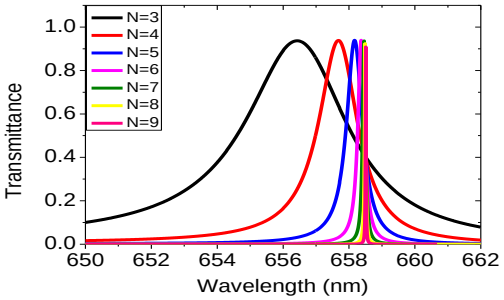

Fig. 18. Transmission spectra of a quaternary photonic crystal for different number of periods at n_1 = 4.23, n_2 = 3.4, n_3 = 2.0, n_4 = 1.37, θ_0 = 0.0°, d_f = 1D and the defect layer position is P1.

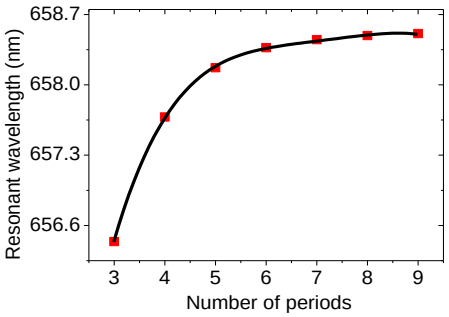

Fig. 19. Resonant wavelength of the defect mode as a function of the number of periods at n_1 = 4.23, n_2 = 3.4, n_3 = 2.0, n_4 = 1.37, θ_0 = 0.0°, d_f = 1D and the defect layer position is P1.

Table 4. Resonant wavelength, full width at half maximum, quality factor and maximum transmittance of the defect mode for different values of the number of periods.

Number of periods	Resonant wavelength (nm)	FWHM (nm)	Quality factor	Maximum transmittance
3	656.44	3.8	172.74	0.93
4	657.68	1.46	450.46	0.93
5	658.17	0.60	1096.95	0.93
6	658.37	0.25	2633.48	0.93
7	658.45	0.11	5985.90	0.93
8	658.49	0.04	16462.25	0.92
9	658.51	0.02	32925.5	0.90

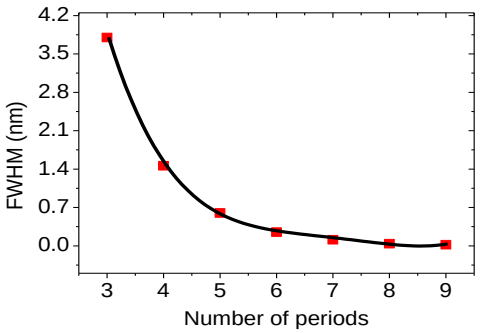

Fig. 20. Full width at half maximum versus the number of periods at $n_1 = 4.23$, $n_2 = 3.4$, $n_3 = 2.0$, $n_4 = 1.37$, $\theta_0 = 0.0°$, d_f = 1D and the defect layer position is P1.

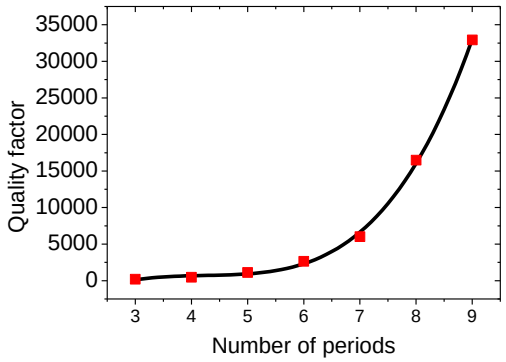

Fig. 21. Quality factor versus the number of periods at $n_1 = 4.23$, $n_2 = 3.4$, $n_3 = 2.0$, $n_4 = 1.37$, $\theta_0 = 0.0°$, d_f = 1D and the defect layer position is P1.

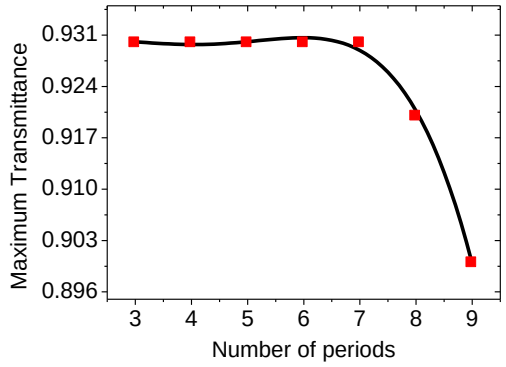

Fig. 22. Maximum transmittance versus the number of periods at $n_1 = 4.23$, $n_2 = 3.4$, $n_3 = 2.0$, $n_4 = 1.37$, $\theta_0 = 0.0°$, d_f = 1D and the defect layer position is P1.

4. Conclusion

A one-dimensional quaternary defective photonic crystal with the structure $(Ge/Si/Si_3N_4/MgF_2)^N$/Defect Layer/$(Ge/Si/Si_3N_4/MgF_2)^N$ has been investigated. The transfer matrix method has been used to analyze the transmission spectra through the proposed structure. The defect mode properties such as wavelength position, full width at half maximum, quality factor and maximum transmittance have been investigated. It is found that these properties are sensitive to the incident angle, defect layer position, defect layer thickness and the number of periods. Many interesting findings are observed such as an angle of incidence of 85°, a defect layer thickness of 400 nm and a number of periods of 9 can be considered as optimum parameters since they correspond to the highest quality factor, the lowest full width at half maxim and a maximum of transmittance of about unity. The proposed photonic crystal can be used as a tunable filter. It can also be employed in the field of optical sensing. It can be used as a biosensor, chemical sensor and refractometric sensor.

References

[1] S.G. Shafagh, H. Kaatuzian, and M. Danaie, "A highly sensitive tunable filter using hybrid 1-D photonic crystal and plasmonic MIM waveguide", Optik, vol. 228, 166174, 2021.

[2] F. S. Chaves, and H.V. Posada, "Two-dimensional photonic crystals with insertion of circular and triangular defects", Optik, vol. 246, 167830, 2021

[3] Y.G. Ju, "Tolerance analysis of photonic crystal substrate used in spectrometer-free photonic crystal enhanced microscopy", Opt Quant Electron, vol. 52, 485, 2020.

[4] I Z. Baraket, and M Kanzari, "Design of a very optimized ultra-wide magnetic band gap photonic crystal device", Opt Quant Electron, vol. 53, 575, 2021.

[5] P. Sarkar, A. Panda, and G. Palai, "Analysis of 90° bend photonic crystal waveguide: an application to optical interconnect", Indian J Phys, vol. 93, pp. 1495–1500, 2019.

[6] A. Kumar, K.B. Thapa, and S.P. Ojha "A tunable broadband filter of ternary photonic crystal containing plasma and superconducting material", Indian J Phys., vol. 93, pp. 791–798, 2019.

[7] A. Mishra, S. Awasthi, S. Srivastava, U. Malaviya, and S. Ojha, "Tunable and omnidirectional filters based on one-dimensional photonic crystals composed of single-negative materials", J. Opt. Soc. Am. B, vol. 28, pp. 1416-1422, 2011.

[8] F. Xue, S.B. Liu, H.F. Zhang, X.K. Kong, Y.D. Wen, L.L. Wang, and S. Qian, "The theoretical analysis of omnidirectional photonic band gaps in the one-dimensional ternary plasma photonic crystals based on Pell quasi-periodic structure" Opt Quant Electron, vol. 49, 19, 2017.

[9] M. Zoysa, M. Yoshida, B. Song, K. Ishizaki, T. Inoue, S. Katsuno, K. Izumi, Y. Tanaka, R. Hatsuda, J. Gelleta, and S. Noda, "Thermal management for CW operation of large-area double-lattice photonic-crystal lasers", J. Opt. Soc. Am. B, vol. 37, pp. 3882-3887, 2020.

[10] S. Rebhi, and M. Najjar, "Hourglass nonlinear photonic crystal cavity for ultra-fast all-optical switching", Optik, vol. 180, pp. 858-865, 2019.

[11] R.R. Ghosh, P. Bhardwaj, and A. Dhawan, "Numerical modeling of integrated electro-optic modulators based on mode-gap shifting in photonic crystal slab waveguides containing a phase change material", J. Opt. Soc. Am. B, vol. 37, pp. 2287-2298, 2020.

[12] F. Bozorgzadeh, D. Ahmadi, M. Sahrai, "Innovative fiber Bragg grating filter based on a graphene photonic crystal microcavity", Appl. Opt., vol. 59, pp. 84-91, 2020.

[13] Z. Fu, F. Sun, C. Wang, J. Wang, and H. Tian, "High-sensitivity broad free-spectral-range two-dimensional three-slot photonic crystal sensor integrated with a 1D photonic crystal bandgap filter", Appl. Opt., vol. 58, pp. 5997-6002, 2019.

[14] S.A. Taya, O.M. Ramahi, M.A. Abutailkh, N. Doghmosh, Z.M. Nassar, A. Upadhyay, and I. Colak, "Investigation of bandgap properties in one-dimensional binary superconductor–dielectric photonic crystal: TE case", Indian J Phys, vol. 96, pp. 2151-2160, 2022.

[15] N. Doghmosh, S.A. Taya, A. Upadhyay, M.M. Olaimat, and I. Colak, "Enhancement of optical visible wavelength region selective reflector for photovoltaic cell applications using a ternary photonic crystal", Optik, vol. 243, 167491, 2021.

[16] S.A. Taya, N. Doghmosh, Z.M. Nassar, A.A. Alkanoo, and A. Upadhyay, "Properties of a binary photonic crystal with an inverted symmetry and a defect layer", Eur. Phys. J. Plus, vol. 135, 935, 2020.

[17] M.G. Daher, S. A. Taya, I. Colak, D.Vigneswaran, M. M. Olaimat, S. K. Patel, O. M. Ramahi, A. H. M. Almawgani, "Design of a nano-sensor for cancer cell detection based on a ternary photonic crystal with high sensitivity and low detection limit", Chinese Journal of Physics, Vol. 77, Pages 1168-1181, 2022.

[18]M. G. Daher, S. A. Taya, I. Colak, O. M. Ramahi, "Design of a novel optical sensor for the detection of waterborne bacteria based on a photonic crystal with an ultra-high sensitivity", Optical and Quantum Electronics, vol. 54, No. 2, Article number 108, 18 pages, 2022.

[19] M. Taheri, M. Omoomi, and J. Mazloum, "Slow Light Propagation in Photonic Crystal-Based Meandering Delay Lines Using the PTS Material", Arab J Sci Eng, vol. 44, pp. 2335–2343, 2019.

[20] A. Ghanbari, A. Sadr, and H.T. Hesari, "Modeling Photonic Crystal Fiber for Efficient Soliton-Effect Compression of Femtosecond Optical Pulses at 850 nm", Arab J Sci Eng, vol. 39, pp. 3917–3923, 2014.

[21] L. Shi, W. Zhang, J. Jin, Y. Huang, and J. Peng, "Quaternary One-Dimensional Photonic Crystal Cladding Hollow-Core Bragg Fiber", in CLEO:2011 - Laser Applications to Photonic Applications, OSA Technical Digest (CD) (Optica Publishing Group, 2011), paper CThM4.

[22] S. R. Entezar, and A. Rashidi, "Phase Properties of One-Dimensional Quaternary Photonic Crystals", Int. J. Opt. Photonics, vol. 8, pp. 67-72, 2014

[23] V. K. Singh, S. Srivastava, and I. Vibhu, "Study of transmittance spectra for quaternary periodic structure of 1D photonic crystal for s-wave filter", Indian J. Sci Technol, vol. 13, pp. 1580-1588, 2020.

[24] N. J. Bianchi, "Optical properties of one dimensional quaternary photonic crystal and associated heterostructures" Doctor of philosophy dissertation, University of Rhode Island, Open Access Dissertations, Paper 1146. (2020).

[25] A.H. Aly, and Z.A. Zaky, "Ultra-sensitive photonic crystal cancer cells sensor with a high-quality factor", Cryogenics, vol. 104, 102991, 2019.